

Complex scaling of the hyper-spheric coordinates and Faddeev equations

D.V. Fedorov^a, E. Garrido^b, A.S. Jensen^a

^a Department of Physics and Astronomy, Aarhus University, DK-8000 Aarhus C, Denmark

^b Instituto de Estructura de la Materia, CSIC-Serrano 123, E-28006, Madrid, Spain

Abstract. We implement complex scaling of Faddeev equations using hyper-spheric coordinates and adiabatic expansion. Complex scaling of coordinates allows convenient calculations of three-body resonances. We derive the necessary equations and investigate the adiabatic spectrum at large distances. We illustrate the viability of the implementation by calculations of several three-body resonances: a 0^+ resonance in a model benchmark system of three identical bosons; the 2^+ resonance in the ${}^6\text{He}$ nucleus within the $\alpha + n + n$ model; and the two 0^+ resonances in ${}^{12}\text{C}$ within the three- α model.

1 Introduction

Although the quantum-mechanical three-body problem has a long history [1] it is still generally considered as “difficult”. Recently an effective symbiotic method was introduced [2] where the Faddeev equations [3] are solved using the hyper-spheric adiabatic expansion [4]. The method allows analytic asymptotic solutions and thus is especially suitable to describe weakly bound and spatially extended systems. During the last years it has been successfully employed to investigate ground state properties and fragmentation reactions of three-body halo nuclei ${}^6\text{He}$ and ${}^{11}\text{Li}$ [5, 6, 7].

Investigation of three-body systems in basically all fields of physics led very soon to the question of the three-body continuum spectrum. Investigations of three-body resonances is today a hot topic in both experimental and theoretical physics.

In the early 70’s the complex scaling method was introduced [8, 9] to calculate resonances, where the radial coordinate, and therefore the Hamiltonian, is rotated into the complex plane. This transformation does not change the energies of the bound states, while resonances appear as additional bound states with complex energy values. Thus the usual numerical techniques used to compute bound states can also be employed to calculate resonances [10, 11, 12, 13] (see also [14, 15, 16, 17] for recent applications to three-body systems).

A popular alternative coordinate space method to calculate resonances is the complex energy method where the poles of the S -matrix are searched for. This method requires matching of the calculated wave function with a certain large distance asymptotics, typically a Bessel function, but sometimes a more complicated function. Furthermore the asymptotic functions diverge exponentially, and an accurate calculation at large distances becomes soon a delicate numerical task, especially for the long-range Coulomb potentials [18].

The great advantage of the complex scaling method is that it is possible to avoid matching at large distances and to employ instead a simpler boundary condition of vanishing wave function or, alternatively, a basis of square integrable functions.

In this paper we implement the complex scaling method within the hyper-spheric adiabatic approach to the Faddeev equations. We first derive the necessary equations and investigate the asymptotic adiabatic spectrum. We then illustrate the viability of the method by applications to three systems: i) a model benchmark system of three bosons; ii) the halo nucleus ${}^6\text{He}$ within the three-body $\alpha + n + n$ model; and iii) the three- α system where the long range Coulomb interaction is of importance.

2 Complex scaling of hyper-spheric coordinates

In this chapter we reintroduce some pertinent definitions from the complex scaling and hyper-spheric adiabatic methods, perform the scaling of hyper-spheric coordinates, derive the formulae necessary for the numerical implementation of the method, and discuss the large-distance asymptotics of the hyper-angular adiabatic spectrum.

2.1 Complex scaling in a two-body system

A resonance or, in the stationary scattering language, a decaying meta-stable state corresponds to a pole $k_0 = q - i\gamma$ of the S -matrix located in the IV-th quadrant of the complex momentum. The corresponding radial wave-function f_{k_0} asymptotically grows exponentially

$$f_{k_0} \propto e^{iqr} e^{\gamma r}. \quad (1)$$

The complex scaling method is designed to avoid this exponential growth by scaling the coordinate r with a complex exponent $e^{i\theta}$

$$r \rightarrow r e^{i\theta}. \quad (2)$$

This changes the asymptotics (1) of the radial wave-function into

$$f_{k_0} \propto e^{i|k_0|r \cos(\theta - \varphi)} e^{-|k_0|r \sin(\theta - \varphi)}, \quad (3)$$

where $-\varphi$ is the argument of the complex momentum k_0 ($k_0 = |k_0|e^{-i\varphi}$). If $\theta > \varphi$ this wave-function is exponentially vanishing and the resonance effectively becomes a bound state and thus numerical methods designed for bound state problems could also be employed for resonances.

The exponentially vanishing wave-function (3) allows a simple bounding box boundary condition

$$f(r_{\max}) = 0, \quad (4)$$

provided r_{\max} is sufficiently large. The continuum spectrum solution for the complex scaled radial function at large distances is

$$f(r) \propto \sin(kr e^{i\theta} + \delta), \quad (5)$$

where δ is the phase shift. The boundary condition (4) with this function then leads to a trade-mark rotated spectrum of the continuum states lying along a line rotated by $-\theta$ (-2θ in the energy plane)

$$k_n \simeq \frac{\pi n}{r_{\max}} e^{-i\theta}, \quad n = 1, 2, \dots \quad (6)$$

Although the wave-function (3) is exponentially vanishing, the fall-off rate is controlled by the parameter $\sin(\theta - \varphi)$ and therefore r_{\max} must satisfy

$$|k_0|r_{\max} \sin(\theta - \varphi) \gg 1, \quad (7)$$

and thus is typically larger than for bound states, where only

$$|k_0|r_{\max} \gg 1 \quad (8)$$

is needed. Also for exponential, $\exp(-r/b)$, and gaussian, $\exp(-r^2/b^2)$, potentials the range b of the potential is increased after complex scaling as, correspondingly, $b/\cos\theta$ and $b/\sqrt{\cos 2\theta}$. For gaussian potentials the scaling angle therefore can not exceed $\theta = \pi/4$.

This increase of the range of the scaled potential is counterproductive as it necessitates numerical calculations to larger distances.

2.2 Hyper-spheric adiabatic approach

We first define the usual Jacobi coordinates \mathbf{x}_i and \mathbf{y}_i in terms of masses m_i and coordinates \mathbf{r}_i of the three particles ($i=1,2,3$)

$$\mathbf{x}_i = \sqrt{\mu_i}(\mathbf{r}_j - \mathbf{r}_k), \quad (9)$$

$$\mathbf{y}_i = \sqrt{\mu_{(jk)i}} \left(\mathbf{r}_i - \frac{m_j \mathbf{r}_j + m_k \mathbf{r}_k}{m_j + m_k} \right), \quad (10)$$

$$\mu_i = \frac{1}{m} \frac{m_j m_k}{m_j + m_k}, \quad \mu_{(jk)i} = \frac{1}{m} \frac{m_i(m_j + m_k)}{m_i + m_j + m_k}$$

where $\{i, j, k\}$ is a cyclic permutation of $\{1, 2, 3\}$ and m is an arbitrary mass. The hyper-radius ρ and the hyper-angles α_i are now defined as

$$\rho \sin(\alpha_i) = x_i, \quad \rho \cos(\alpha_i) = y_i. \quad (11)$$

A set of hyper-spheric coordinates consists of the hyper-radius ρ and a set of five angles Ω_i – the hyper-angle α_i and the four directional angles of \mathbf{x}_i and \mathbf{y}_i . Here i distinguishes different sets of Jacobi coordinates.

The kinetic energy operator T is then given as

$$T = T_\rho + \frac{\hbar^2}{2m\rho^2} \Lambda^2, \quad (12)$$

$$T_\rho = -\frac{\hbar^2}{2m} \left(\rho^{-5/2} - \frac{\partial^2}{\partial \rho^2} \rho^{5/2} - \frac{1}{\rho^2} \frac{15}{4} \right), \quad (13)$$

$$\Lambda^2 = -\frac{1}{\sin(2\alpha_i)} \frac{\partial^2}{\partial \alpha_i^2} \sin(2\alpha_i) - 4 + \frac{l_{x_i}^2}{\sin^2(\alpha_i)} + \frac{l_{y_i}^2}{\cos^2(\alpha_i)}, \quad (14)$$

where \mathbf{l}_{x_i} and \mathbf{l}_{y_i} are the angular momentum operators related to \mathbf{x}_i and \mathbf{y}_i .

The hyper-spheric adiabatic method allows effective solution of the three-body problem with the Hamiltonian

$$H = T_\rho + \frac{\hbar^2}{2m\rho^2} \Lambda^2 + \sum_{i=1}^3 V_i, \quad (15)$$

where V_i is the two-body potential between particles j and k . The coordinates are divided into the "slow" hyper-radius ρ and "fast" hyper-angles Ω (here we refer to any of the three sets of angles). For every fixed hyper-radius the eigenvalue problem

$$\left[\Lambda^2 + \frac{2m\rho^2}{\hbar^2} \sum_{i=1}^3 V_i \right] \Phi_n = \lambda_n \Phi_n, \quad (16)$$

is solved and the eigenvalues $\lambda_n(\rho)$ and eigen-functions $\Phi_n(\rho, \Omega)$ are calculated as function of ρ . The total wave-function Ψ is then expanded in terms of these eigen-functions

$$\Psi = \frac{1}{\rho^{5/2}} \sum_n f_n(\rho) \Phi_n(\rho, \Omega). \quad (17)$$

The expansion coefficients $f_n(\rho)$ satisfy a coupled system of differential equations where the angular eigenvalues serve as effective potentials

$$\left[-\frac{\partial^2}{\partial \rho^2} + \frac{\lambda_n + 15/4}{\rho^2} - \frac{2mE}{\hbar^2} \right] f_n = \sum_{n'} \left[2P_{nn'} \frac{\partial}{\partial \rho} + Q_{nn'} \right] f_{n'}, \quad (18)$$

where E is the three-body energy and P and Q are the non-adiabatic terms defined as

$$\begin{aligned} P_{nn'}(\rho) &= \int \Phi_n^\dagger(\rho, \Omega) \frac{\partial}{\partial \rho} \Phi_{n'}(\rho, \Omega) d\Omega, \\ Q_{nn'}(\rho) &= \int \Phi_n^\dagger(\rho, \Omega) \frac{\partial^2}{\partial \rho^2} \Phi_{n'}(\rho, \Omega) d\Omega, \end{aligned} \quad (19)$$

where \dagger denotes hermitian conjugation.

2.3 Scaling of hyper-spheric coordinates

We now perform the complex scaling of the Jacobi coordinates

$$x \rightarrow x e^{i\theta}, \quad y \rightarrow y e^{i\theta}. \quad (20)$$

The hyper-radius ρ is then scaled with the same angle θ while the hyper-angles Ω remain real as they only depend upon ratios of the Jacobi coordinates

$$\rho \rightarrow \rho e^{i\theta}, \quad \Omega \rightarrow \Omega. \quad (21)$$

We shall in the following always maintain real ρ writing the complex rotated variable explicitly as $\rho e^{i\theta}$. The angular eigenvalue problem (16) acquires then complex potentials

$$\left[\Lambda^2 + e^{2i\theta} \frac{2m\rho^2}{\hbar^2} \sum_{i=1}^3 V_i(\rho e^{i\theta}, \Omega) \right] \Phi_n = \lambda_n \Phi_n, \quad (22)$$

and therefore the eigenvalues λ_n and eigen-functions Φ_n also become complex.

We solve the complex-scaled eigenvalue problem (22) by using the hyperspheric harmonics as a basis set [2]. Since the hyper-angles are not affected by the complex scaling these functions remain real. The operator \mathcal{H} at the left hand side of the eigenvalue equation (22),

$$\left[\Lambda^2 + e^{2i\theta} \frac{2m\rho^2}{\hbar^2} \sum_{i=1}^3 V_i(\rho e^{i\theta}, \Omega) \right] \equiv \mathcal{H}, \quad (23)$$

is in this basis a symmetric complex matrix, $\mathcal{H}^T = \mathcal{H}$ (here T denotes transposition). A non-scaled hamiltonian, $\theta = 0$, is a real symmetric matrix, that is a hermitian matrix.

A complex matrix \mathcal{H} has in general different left, χ , and right, Φ , eigenvectors corresponding to a given eigenvalue λ

$$\begin{aligned} \mathcal{H}\Phi &= \lambda\Phi, \\ \chi^\dagger \mathcal{H} &= \lambda\chi^\dagger. \end{aligned} \quad (24)$$

The left χ_n and right $\Phi_{n'}$ eigenvectors corresponding to different eigenvalues λ_n and $\lambda_{n'}$ are orthogonal in the following way

$$\chi_n^\dagger \Phi_{n'} = \delta_{nn'}. \quad (25)$$

For a symmetric matrix there is an apparent connection between the left and right eigenvalues

$$\chi^\dagger = \Phi^T. \quad (26)$$

Therefore for the complex scaled angular eigen-vectors the scalar product rule takes a somewhat unusual form

$$\Phi_n^T \Phi_{n'} = \delta_{nn'}, \quad (27)$$

and thus the hermitian conjugation in the definitions of P and Q in (19) must be substituted by transposition in the case of complex scaling.

The hyper-radial equations (18) remain largely unchanged, but, of course, the eigenvalues λ_n together with the non-adiabatic terms P and Q are now complex.

Similar to the two-body case a three-body resonance corresponds to a pole of the three-body S -matrix at a momentum $\kappa = q - i\gamma$ ($\kappa = \sqrt{2mE/\hbar^2}$). At this point all hyper-radial functions f_n have the diverging asymptotics

$$f_n \propto e^{iq\rho} e^{\gamma\rho}. \quad (28)$$

The complex scaling of the hyper-radius leads in complete analogy to the two-body case to an oscillating and exponentially vanishing resonance function

$$f_n \propto e^{i|k_0|\rho \cos(\theta-\phi)} e^{-|k_0|\rho \sin(\theta-\phi)}, \quad (29)$$

and again the boundary condition

$$f_n(\rho_{max} = 0) \quad (30)$$

leads to the rotated discretized continuum states

$$\kappa_j \simeq \frac{\pi j}{\rho_{max}} e^{-i\theta}, \quad j = 1, 2, \dots. \quad (31)$$

2.4 Faddeev equations.

The angular wave-function Φ is now represented as a sum of three components $\Phi = \phi^{(1)} + \phi^{(2)} + \phi^{(3)}$ which satisfy the three Faddeev equations

$$\Lambda^2 \phi^{(k)} + e^{2i\theta} \frac{2m\rho^2}{\hbar^2} V_k(\rho e^{i\theta}, \Omega) \Phi = \lambda \phi^{(k)}, \quad (32)$$

where $k=1,2,3$. One can easily verify that the sum of these three Faddeev equations is equivalent to the Schrödinger equation (22).

The Faddeev equations (32) can be conveniently written in a matrix form as

$$F\phi = \lambda\phi, \quad (33)$$

where ϕ is a column vector of the three Faddeev components

$$\phi = \begin{pmatrix} \phi^{(1)} \\ \phi^{(2)} \\ \phi^{(3)} \end{pmatrix} \quad (34)$$

and the Faddeev operator F is equal

$$F = T + VR, \quad (35)$$

where T is the kinetic energy matrix

$$T = \begin{pmatrix} \Lambda^2 & 0 & 0 \\ 0 & \Lambda^2 & 0 \\ 0 & 0 & \Lambda^2 \end{pmatrix}, \quad (36)$$

V is the potential matrix

$$V = \begin{pmatrix} V_1 & 0 & 0 \\ 0 & V_2 & 0 \\ 0 & 0 & V_3 \end{pmatrix}. \quad (37)$$

and R is the projection matrix

$$R = \begin{pmatrix} 1 & 1 & 1 \\ 1 & 1 & 1 \\ 1 & 1 & 1 \end{pmatrix}. \quad (38)$$

If we again use hyper-spheric harmonics as a basis set then each of the elements in the above matrices becomes in turn a matrix in this basis.

The matrix R acting on the Faddeev vector (34) apparently produces a vector with the total function Φ as the three components. The matrix R has the following properties

$$\begin{aligned} R^2 &= 3R, \\ R^T &= R \end{aligned} \quad (39)$$

The scalar product rule (27) for the Faddeev functions becomes

$$\begin{aligned} \phi_n^T R^T R \phi_{n'} &= \delta_{nn'} \Rightarrow \\ \phi_n^T R \phi_{n'} &= \frac{1}{3} \delta_{nn'}. \end{aligned} \quad (40)$$

The factor $1/3$ can be hidden into the normalization by redefining the wavefunctions such that

$$\phi_n^T R \phi_{n'} = \delta_{nn'}. \quad (41)$$

This product rule should be used in the definitions (19) of the non-adiabatic terms P and Q if one uses the Faddeev three-component functions:

$$\begin{aligned} P_{nn'}(\rho) &= \int \phi_n^T R \frac{\partial \phi_{n'}}{\partial \rho} d\Omega, \\ Q_{nn'}(\rho) &= \int \phi_n^T R \frac{\partial^2 \phi_{n'}}{\partial \rho^2} d\Omega. \end{aligned} \quad (42)$$

Actually, the product rule with the R -matrix (41) represents the ordinary product rule for the Faddeev operator F . Although the Faddeev matrix is not hermitian, it has the important symmetry property

$$RF = F^T R, \quad (43)$$

which leads to a simple connection between the left, φ , and right, ϕ , eigenvectors of the matrix F

$$\varphi^\dagger = \phi^T R, \quad (44)$$

which immediately leads to (41).

Equation (44) can be proved by multiplying (33) with R from the left, transposing it and using the relation (43). Apparently, since we did not assume that the matrix V is real, the complex scaling does not affect the validity of the above expressions.

Note that for the non-scaled real F the property (43) means that the eigenvalues of F are real although the matrix itself is not hermitian.

2.5 Phase of the angular eigen-functions

The complex eigen-functions Φ_n obtained from the complex scaled eigenvalue equation (22) are as usual defined up to a phase factor. We can therefore multiply the eigen-function Φ_n by an arbitrary phase function $e^{i\chi_n(\rho)}$, where χ_n is real. This changes the non-adiabatic terms P and Q in (19) as

$$P_{nn'} \rightarrow P_{nn'} + i\chi'_{n'}\delta_{nn'}, \quad (45)$$

$$Q_{nn'} \rightarrow Q_{nn'} + 2i\chi'_{n'}P_{nn'} + (i\chi''_{n'} - \chi'^2_{n'})\delta_{nn'}, \quad (46)$$

(where primes denote differentiation with respect to ρ) and correspondingly, via equation (18), leads to different radial functions f_n . However, the total wave-function $\Psi \propto \Phi_n f_n$ in (17) does not change as the new set of radial functions merely corresponds to a trivial phase shift

$$f_n \rightarrow e^{-i\chi_n(\rho)} f_n, \quad (47)$$

such that the product of the angular and the radial function remains unchanged

$$\Phi_n f_n \rightarrow e^{i\chi_n} \Phi_n e^{-i\chi_n(\rho)} f_n = \Phi_n f_n. \quad (48)$$

Indeed the right hand side of the radial equations (18) transforms as

$$e^{-i\chi_n} \left[2P_{nn'} \frac{\partial}{\partial \rho} + Q_{nn'} \right] f_{n'} \rightarrow e^{-i\chi_{n'}} \left(2P_{nn'} \frac{\partial}{\partial \rho} + Q_{nn'} \right) f_{n'} + (\chi'^2_{n'} + i\chi''_{n'}) \delta_{nn'} f_{n'} + 2i\chi'_{n'} \delta_{nn'} \frac{\partial}{\partial \rho} f_{n'} \quad (49)$$

The last two terms, however, precisely cancel with the corresponding terms from the second derivative at the left hand side of the radial equations (18)

$$\frac{\partial^2}{\partial \rho^2} f_n \rightarrow \frac{\partial^2}{\partial \rho^2} e^{-i\chi_n} f_n = e^{-i\chi_n} \left(\frac{\partial^2}{\partial \rho^2} f_n - i\chi''_{n'} f_n - \chi'^2_{n'} f_n - 2i\chi'_{n'} \frac{\partial}{\partial \rho} f_n \right). \quad (50)$$

Thus the phase of the hyper-angular eigen-functions can be chosen arbitrarily as the total wave-function is independent of this phase.

In the non-scaled case the diagonal elements P_{nn} are identically equal zero. It is convenient to chose the phase such that this property holds also for the scaled case. One can easily verify from (45) that the phase

$$\chi_n(\rho) = \exp \left(i \int_0^\rho P_{nn}(\rho') d\rho' \right), \quad (51)$$

precisely leads to a vanishing diagonal P as in the non-complex-scaled case.

The freedom in choosing the phase can also be exploited in order to eliminate a given non-diagonal term $Q_{nn'}$. The phase should in this case instead be chosen as

$$\chi_{n'}^{(n)}(\rho) = \exp \left(\frac{i}{2} \int_0^\rho P_{nn'}^{-1}(\rho') Q_{nn'}(\rho') d\rho' \right), \quad (52)$$

as seen from (46).

2.6 Asymptotics of the eigenvalues

In the angular eigenvalue problem (22) the two-body potentials are multiplied by ρ^2 . At the origin, $\rho=0$, they therefore vanish from the equations and the eigenvalues then start from the free spectrum $K(K+4)$, where K is even or odd integer. The next term in the ρ expansion is proportional to ρ^2 as in the non-scaled case [2].

The large distance asymptotics can be investigated by use of zero-range potentials. For our purpose it is also sufficient to assume that only one pair of particles interact with each other. This simple model will show all different types of asymptotics except for the Efimov effect [19]. However the latter is not the subject of the current investigation.

In this case the physical (non-spurious [2]) solution to the Faddeev equations (32) contains only one non-zero Faddeev component in (34), namely the one where the two-body potential acts.

The zero-range potential is vanishing everywhere except for the origin. The physical (one-component) solution to the equation (32) is then a simple function

$$\phi = \sin(\nu(\alpha - \frac{\pi}{2})), \quad (53)$$

where $\nu = \sqrt{\lambda + 4}$. The zero range potential enters as a boundary condition at the origin [20]

$$-\nu \frac{\cos(\nu \frac{\pi}{2})}{\sin(\nu \frac{\pi}{2})} = \frac{1}{\sqrt{\mu}} \frac{\rho}{a} e^{i\theta}, \quad (54)$$

where μ is the reduced mass of two particles in units of m , and a is the two-body scattering length¹.

For $\rho \gg |a|$ this equation has several types of solutions. First there is a series of asymptotic solutions where $\sin(\nu \frac{\pi}{2})$ is zero

$$\nu_n = 2n, \quad \lambda_n = (2n)^2 - 4, \quad n = 1, 2, \dots \quad (55)$$

which is the free hyper-spheric spectrum $K(K+4)$ with $K = 2n - 2$.

Another type of solution may exist when $\cot(\nu \frac{\pi}{2})$ remains finite but the complex quantity ν instead is proportional to ρ . Suppose that the scattering length is negative, $a < 0$, corresponding to a bound two-body state with binding energy $B = \hbar^2/(2m\mu a^2)$. In this case there exists an asymptotic solution to (54)

$$\nu = \frac{1}{\sqrt{\mu}} \frac{\rho}{a} e^{i(\theta + \pi/2)}, \quad (56)$$

since in this case $\cot(\nu \frac{\pi}{2}) \rightarrow i$.

Therefore a bound two-body state always results in an asymptotically quadratically diverging eigenvalue $\lambda = \nu^2 - 4$

$$\lambda = -\frac{2mB}{\hbar^2} \rho^2 e^{2i\theta}. \quad (57)$$

For positive scattering length, $a > 0$ and $\theta < \pi/2$ only the free asymptotic solutions (55) to the equation equation (54) exist. Positive scattering length

¹The sign convention for the scattering length is $k \cot(\delta) = 1/a + O(k^2)$

corresponds to a resonance (more precisely a virtual state) which is located at the complex momentum $k = -i/a$, that is with the argument $-\pi/2$ in the complex momentum plane. The energy of the virtual state is given by $E_0 = -\hbar^2/(2m\mu a^2)$.

When $a > 0$ and the scaling angle θ is larger than $\pi/2$ yet additional asymptotic solution to (54) appears

$$\nu = \frac{1}{\sqrt{\mu}} \frac{\rho}{a} e^{i(\theta-\pi/2)}. \quad (58)$$

That is when the scaling angle θ is larger than the angle of a resonance ($\pi/2$ in the case of a virtual state) the latter effectively becomes a bound state resulting in an angular eigenvalue similar to (57) but with the resonance (or virtual state) energy E_0 instead of the bound state energy

$$\lambda = \frac{2mE_0}{\hbar^2} \rho^2 e^{2i\theta}. \quad (59)$$

Thus the asymptotic spectrum of hyper-angular eigenvalues primarily consists of the free spectrum (55). In addition each two-body bound state gives a quadratically diverging eigenvalue (57), and finally each two-body resonance (or virtual state) whose argument is less the scaling angle θ also provides a quadratically divergent eigenvalue (59).

The eigenvalues enter the hyper-radial equations (18) as effective potentials λ/ρ^2 . After divided by ρ^2 the free eigenvalues (55) converge to the three-body threshold at zero energy. These eigenvalues asymptotically describe the genuine three-body states where all three particles are away from each other. The eigenvalues (57) corresponding to the two-body bound state after division by ρ^2 converge to a lower threshold at the energy of the two-body bound state. These eigenvalues asymptotically describe a configuration where two of the particles are in the two-body bound state while the third particle is in the continuum. Finally, the two-body resonances and virtual states which after complex scaling appear as bound states produce the same type of asymptotic solutions as the true bound states.

3 Numerical examples

In this chapter we investigate several resonances in different three-body systems using the formulated complex-scaled hyper-spheric method and compare with other methods. The first application is a benchmark calculation of a resonance in a model three-boson system [15] with short-range potentials. The second is a narrow 2^+ resonance in the halo nucleus ^6He . The third application is the two lowest 0^+ resonances in a system of three α -particles where the long-range Coulomb forces are particularly important.

First we solve the angular eigenvalue problem (22) by expansion in hyper-spheric harmonics and obtain thereby several of the lowest eigenvalues $\lambda_n(\rho)$ as functions of ρ . For the system of radial equations (18) we employ the finite difference method. A mesh of about 100 points in hyperradius from zero to a certain maximal distance ρ_{max} is chosen such that the density of points is highest in the regions were the non-adiabatic terms P and Q contribute most.

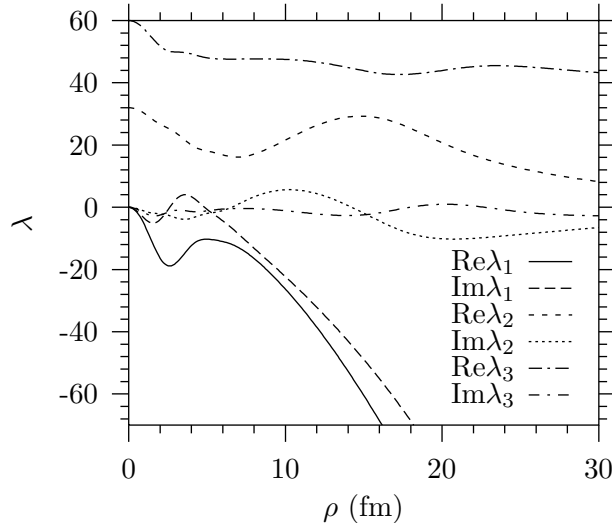


Figure 1. The three lowest complex angular eigenvalues for the model system of three identical bosons with scaling angle $\theta=0.35$.

We then approximate the second and first derivatives in (18) by a five point finite difference approximation assuming that the radial functions are zero at the origin and at ρ_{max} . The system of differential equations (18) then turns into a complex-matrix diagonalization problem. Numerical diagonalization of the matrix gives the complex eigenvalues which include all bound states, resonances and also discretized continuum states. The resulting eigenvectors give the values of radial functions at the mesh points.

The shooting method with direct Runge-Kutta integration of the radial equations gives a better precision but requires a separate search for each of the complex eigenvalues. Thus the preferred strategy could be first to get an overall picture of the complex spectrum by the finite difference method and then to calculate selected eigenvalues with higher precision by the shooting method.

For each of the following examples we show the angular eigenvalues, the complex energy spectrum and the hyper-radial functions of the resonances. As these calculations only serve the purpose of illustration we have not optimized the hyper-radial mesh to achieve the maximum accuracy. With about 100 hyper-radial points the accuracy is about 10 keV in the complex energy.

3.1 A model three-body system

In reference [15] a resonance has been calculated in a model three-body system of identical bosons with the nucleon mass. The model potential acts only on the s-waves and consists of a gaussian attractive pocket and a barrier

$$V(r) = -55\text{MeV} \exp(-0.2\text{fm}^{-2}r^2) + 1.5\text{MeV} \exp(-0.01\text{fm}^{-2}(r - 5\text{fm})^2).$$

A three-body resonance was found in [15] at $E = -5.9525 - 0.4034i$ MeV by solving two-dimensional equations.

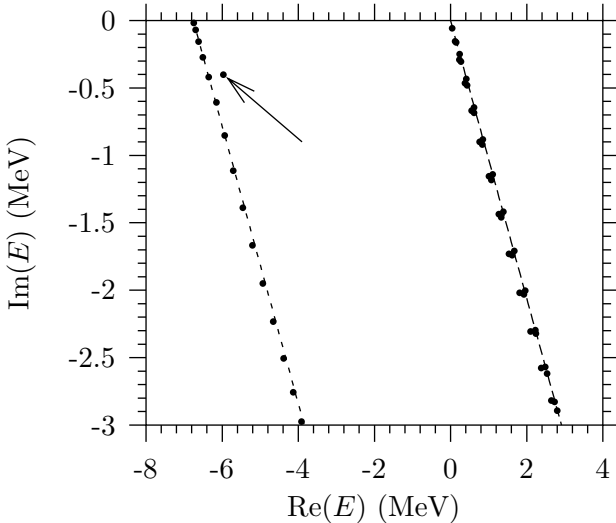


Figure 2. The complex energy spectrum of the model three-boson system with scaling angle $\theta=0.4$. The bound state at $E = -37.22$ MeV is not shown. The resonance at $E = -5.96 - 0.40i$ MeV is indicated by an arrow. The two lines, $\text{Im}(E) = -\tan(2\theta)\text{Re}(E)$ and $\text{Im}(E) = -\tan(2\theta)(\text{Re}(E) - E^{(2)})$ (where $E^{(2)} = -6.76$ MeV is the two-body bound state energy), represent the exact rotated continuum spectrum.

In our calculation we adopt the nucleon mass $m=939$ MeV as the mass unit and use $\hbar c=197.3$ MeV fm. The three lowest angular eigenvalues obtained by solving equation (22) for the complex scaling angle $\theta=0.4$ are shown on Fig. 1. At the origin the three lowest eigenvalues are real and equal to 0, 32 and 60 which correspond to a free hyper-spheric real spectrum of $K(K+4)$ with $K = 0, 4, 6$. The number $K=2$ is forbidden by the bosonic symmetry requirement.

At large distances the lowest eigenvalue diverges quadratically according to (57) due to a bound two-body state. The other eigenvalues return back to the free real spectrum at large distances with one of them taking the place of the diverged lowest eigenvalue.

The energy spectrum for this model system is shown on Fig. 2. The points which form two lines represent the discretized continuum spectrum. The line which starts from $E=0$ corresponds to the states with genuine three-body asymptotics where all three particles are at the continuum. Another line which starts at the two-body bound state energy $E^{(2)} = -6.76$ MeV corresponds to the continuum states where two of the particles are confined in the bound two-body state while the third one is in the continuum.

Using four angular eigenvalues and $\rho_{\max} \sim 100$ fm we find a bound three-body ground state at $E_0 = -37.22$ MeV and a resonance at $E_1 = -5.96 - 0.40i$ MeV in agreement with [15]. The independence of the calculated energies upon the scaling angle is illustrated in Table 1.

The radial function for the resonance is shown on Fig. 3. At shorter distances the function looks like a bound first excited state as indicated by the single node in the real part at shorter distances. At larger distances though, unlike the bound

Table 1. The ground state energy E_0 and the resonance energy E_1 for different scaling angles θ for the model system

θ	E_0 , MeV	E_1 , MeV
0.30	-37.221	$-5.968 - 0.400i$
0.35	-37.220	$-5.962 - 0.404i$
0.40	-37.221	$-5.963 - 0.401i$

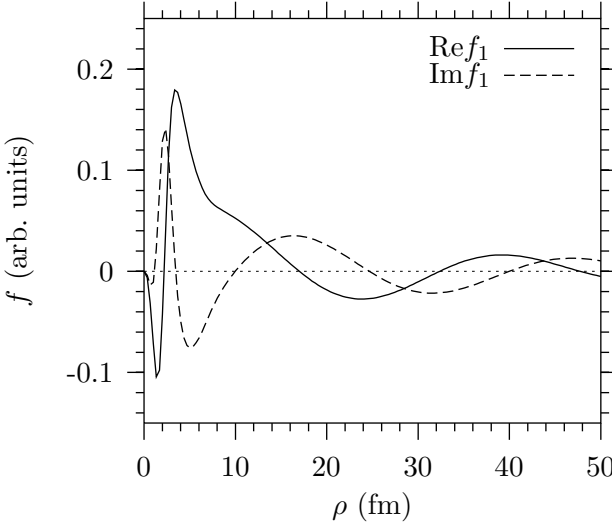


Figure 3. The dominating hyper-radial function f_1 of the lowest resonance in the model three-boson system. The scaling angle is $\theta=0.4$.

state functions, the resonance function oscillates with decreasing amplitude due to the complex scaling in accordance with (3).

3.2 Application to ${}^6\text{He}$

In this section we apply the complex scaled adiabatic hyper-spheric method to the 2^+ resonance in the halo nucleus ${}^6\text{He}$ within the three-body $\alpha+n+n$ model.

We use the same interactions as in [21], namely gaussian potentials fitted to the low energy scattering data and a phenomenological gaussian three-body force. This force is introduced to account for the additional polarisation of the alpha particle due to the presence of another neutron. It simulates the small additional attraction in $\alpha + n + n$ coming from excitations of the α -particle. The mass of the α -particle is assumed to be 4×939 MeV.

The four lowest angular eigenvalues are shown on Fig. 4 for the scaling angle $\theta=0.2$. The eigenvalues start at $\rho=0$ from the real numbers 12 and 32 which correspond to the free real hyper-spheric spectrum of $K(K+4)$ with the hyper-angular momentum $K=2$ and 4. One of the eigenvalues then forms an attractive pocket where the resonance resides. This is largely due to $n-\alpha$ p -waves where the potential is attractive. The other two eigenvalues relate to $n-\alpha$ s -waves with strong repulsion which leads to the two repulsive eigenvalues contributing much

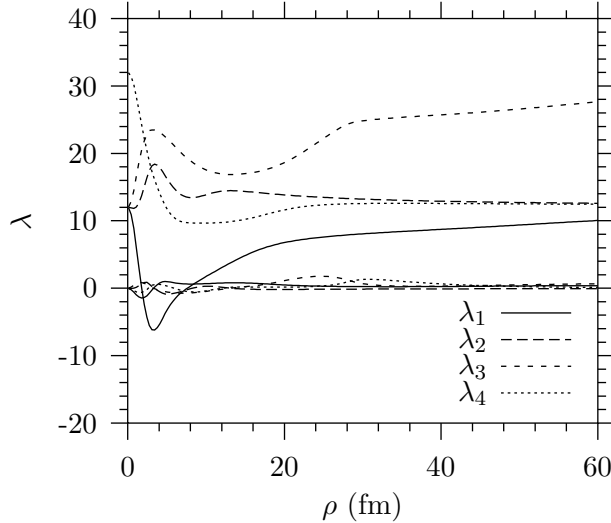


Figure 4. The four lowest complex eigenvalues for the $\alpha+n+n$ system, $J^\pi=2^+$. The scaling angle is $\theta=0.2$.

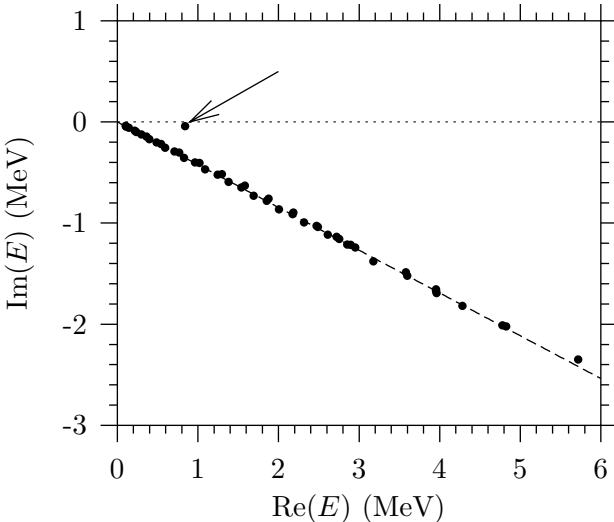


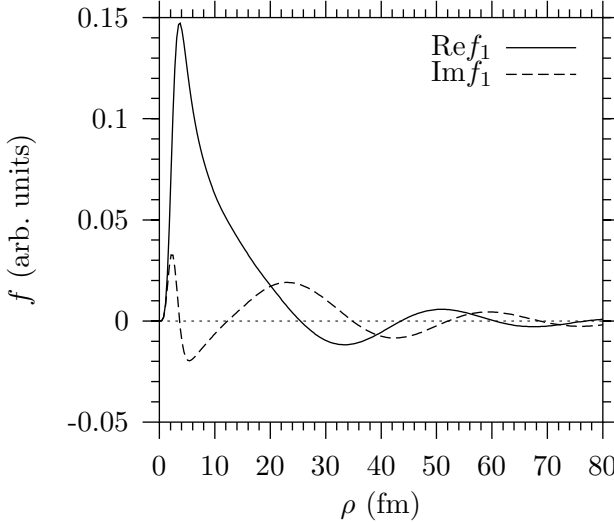
Figure 5. The complex energy spectrum of ${}^6\text{He}$ 2^+ states for the scaling angle $\theta=0.2$. The resonance at $E = 0.842 - 0.041i$ MeV is indicated by an arrow. The line $\text{Im}(E) = -\tan(2\theta)\text{Re}(E)$ represents the exact rotated continuum spectrum.

less to the resonance wave-function. At large distances the eigenvalues return back to the free real spectrum as there are no two-body bound states in this system and the scaling angle is too small for the two-body resonances to become bound.

The complex scaled spectrum for 2^+ states in ${}^6\text{He}$ is shown on Fig. 5. No bound three-body states but one narrow resonance are present with these quantum numbers. With four adiabatic channels and $\rho_{\max} \sim 100$ fm we obtain the 2^+ resonance at $E = 0.842 - 0.041i$ MeV which is reasonably close to the re-

Table 2. Resonance energy E for different scaling angles θ for the $\alpha + n + n$ system

θ	E , MeV
0.15	$0.8419 - 0.0405i$
0.20	$0.8417 - 0.0404i$
0.25	$0.8416 - 0.0405i$

**Figure 6.** The dominating hyper-radial function f_1 of the $\alpha+n+n$ system for the $J^\pi = 2^+$ resonance for the scaling angle $\theta=0.2$.

sult $E = 0.845 - 0.046i$ MeV obtained in [21] with the complex energy method and $\rho_{max}=180$ fm. A similar result, $E = 0.81 - 0.065i$, has been obtained in [16], also with complex scaling method but with a different interaction model. The independence of the resonance energy on the scaling angle is illustrated in Table 2.

The largest hyper-radial function of the resonance is shown on Fig. 6. In the inner region the hyper-radial function resembles a bound ground state function with no nodes and a considerable concentration in the pocket region. Again we see a fingerprint of a complex scaled resonance, namely the wave-function oscillating at large distances with ever decreasing amplitude according to (29).

3.3 Application to the three- α system

The narrow 0^+ resonance in ^{12}C nucleus with $E = 0.38$ MeV and $\Gamma = 8.3 \pm 1.0$ eV was described quantitatively in [18] within a three- α model using the complex energy method. Here we repeat the calculation using the same parameters but instead with the complex scaling method. Unlike the first two numerical examples this one now includes a long range Coulomb potential which significantly alters the asymptotics of the wave-function [18] compared to short range potentials.

The α - α potential is taken as in [18]

$$V(r) = (125\text{MeV} \hat{P}_{l=0} + 20\text{MeV} \hat{P}_{l=2}) e^{-r^2/(1.53\text{fm})^2}$$

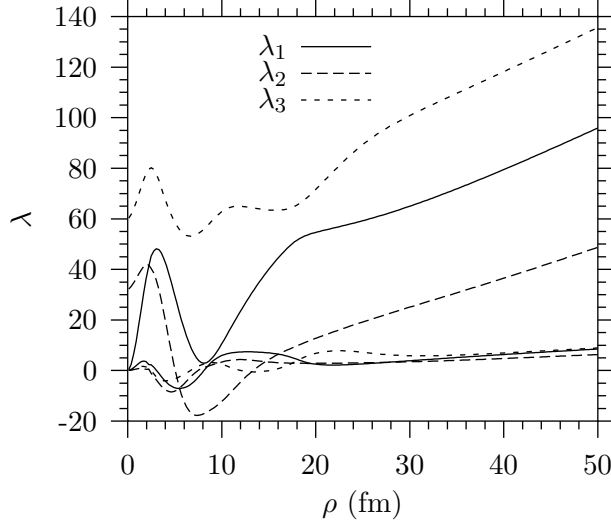


Figure 7. The three lowest complex scaled angular eigenvalues for the three- α system. The scaling angle $\theta=0.11$.

$$- 30.18 \text{ MeV} e^{-r^2/(2.85 \text{ fm})^2}, \quad (60)$$

where \hat{P}_l is the projection operator onto a state with relative orbital momentum l . The three-body force is $V_3(\rho) = -96.8 \text{ MeV} \exp(-\rho^2/(3.9 \text{ fm})^2)$ where the nucleon mass $m=939 \text{ MeV}$ was used as a scale in the definition (10-11) of the hyper-radius ρ .

The angular eigenvalues for this system are shown on Fig. 7. The lowest eigenvalue starts from zero corresponding to $K = 0$. It contains mostly repulsive s-waves and is always positive without any attractive pocket. The next eigenvalue starts from $\lambda=32$ ($K = 4$) as the hyper-angular quantum number $K = 2$ is forbidden by symmetry requirements. It contains mostly attractive p-waves and does form a relatively deep attractive pocket.

At large ρ the real and imaginary parts of the eigenvalues grow linearly instead of converging to a real constant as is the case with short range potentials. This linear growth is due to the long range Coulomb potential [18] which reappears in the effective potentials after the eigenvalue is divided by ρ^2 .

The energy spectrum is shown on Fig. 8 for the scaling angle $\theta=0.1$ and $\rho_{max}=60 \text{ fm}$. There is a bound ground state located at $E_0 = -6.79 \text{ MeV}$ and two resonances, the very narrow one at $E_1 = 0.330 \text{ MeV}$ and a broader resonance at $E_2 = 4.30 - 0.32i \text{ MeV}$.

It is somewhat difficult to tell the first resonance from a discretized continuum state judging from the energy spectrum plot alone. However the hyper-radial wave-function shown on Fig. 9 leaves no doubts that this is indeed a resonance. Shown is the dominating function f_2 which corresponds to the second eigenvalue on Fig. 7 where the attractive pocket is present. The function is again concentrated at smaller distances and has one node in the real part corresponding to the first excited state. At larger distances it basically falls off without oscillations like as if it were a true bound state. This behavior results from the large effective

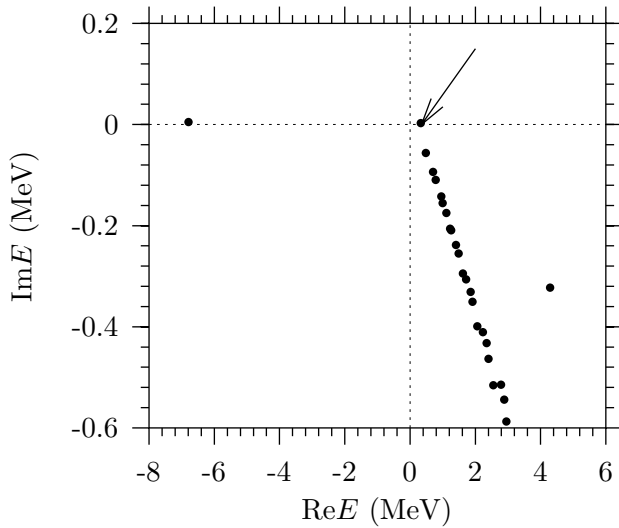


Figure 8. The complex energy spectrum of the three- α 0^+ states for the scaling angle $\theta=0.11$. The resonance at $E = 0.33$ MeV is indicated by an arrow.

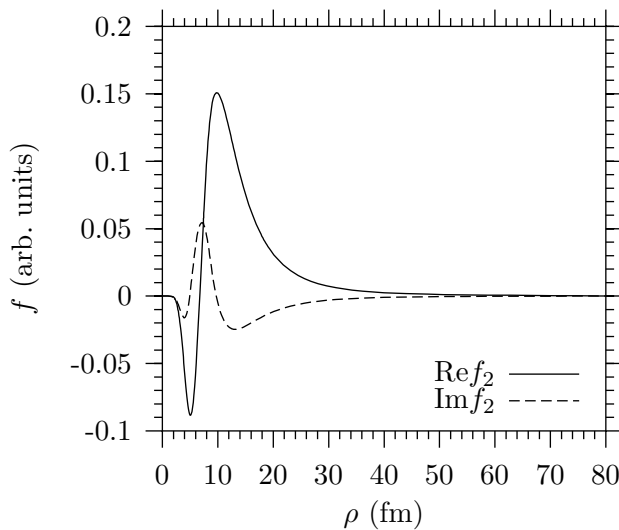


Figure 9. The dominating hyper-radial function $f_2(\rho)$ for the three- α system for the lowest 0^+ resonance and $\theta=0.11$.

Table 3. The bound state energy E_0 and resonance energies E_1 and E_2 of the three lowest 0^+ states in 3α system

θ	E_0 , MeV	E_1 , MeV	E_2 , MeV
0.11	-6.789	0.3300	$4.295 - 0.323i$
0.12	-6.793	0.3283	$4.294 - 0.323i$
0.13	-6.790	0.3297	$4.296 - 0.325i$
0.14	-6.790	0.3296	$4.300 - 0.321i$

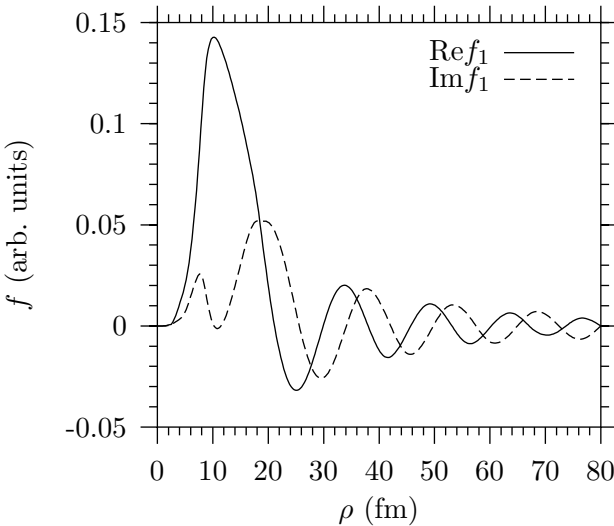


Figure 10. The dominating hyper-radial function $f_1(\rho)$ for the three- α system for the second 0^+ resonance and $\theta=0.11$.

Coulomb barrier provided by the linearly growing angular eigenvalues as shown on Fig. 7.

Another criterion to distinguish the resonances from the continuum states is that when the scaling angle θ is changed the whole line of continuum states rotates according to (31) while the resonances (and bound states) are independent of the scaling angle as illustrated in Table 3.

The energies obtained in this calculation compare well to the values of -6.81 MeV for the ground state and 380-0.02*i* keV for the first resonance obtained in [18] with the complex-energy method. The source of the difference is that in [18] only two of the lowest angular eigenvalues were used while here we use as many eigenvalues as needed for convergence – typically 4-5. Again for these numerical illustrations we have more or less arbitrarily chosen about 100 mesh points in the hyperradius for all examples. No fine tuning has been made in order to achieve higher accuracy. The present numerical error is estimated to be about 10 keV and, therefore, the width of the order of 0.01 keV of the first extremely narrow resonance is beyond the capabilities of an untuned mesh.

Another resonance, which was not calculated in [18], is clearly seen in the spectrum with the energy $E = 4.30 - 0.32i$ MeV, that is with the excitation energy $E^*=11$ MeV and the width $\Gamma=0.6$ MeV. It apparently corresponds to the

experimentally known broader second excited 0^+ state with $E^*=10.3\pm0.3$ MeV and $\Gamma=3\pm0.7$ MeV [22].

The dominating radial function, which for this resonance corresponds to the first eigenvalue on Fig. 7, is shown on Fig. 10. The real part of the wavefunction has no nodes in the pocket region. Therefore this resonance represents the lowest state in the hyper-angular eigenvalue number 1. This eigenvalue also forms a pocket, see Fig. 7, although not as deep as that of eigenvalue number 2.

4 Conclusion

We have implemented complex scaling of coordinates within the hyper-spheric adiabatic approach to Faddeev equations. We have derived the necessary equations and investigated the asymptotic spectrum of the hyper-angular eigenvalues.

The complex-scaled hyper-radial wave-functions fall off exponentially at large distances which allows the simple boundary condition of vanishing functions to be used in the search for the resonances. Alternatively, it is possible to use square integrable functions as a basis set, thus avoiding the less effective shoot-and-match method. Using such a basis expansion has an additional advantage that all bound states and resonances are calculated in one diagonalization run while otherwise one has to search separately for every single pole of the S-matrix. Again with basis expansion in addition to resonances and bound states one also gets in the same run the (discretized) continuum wave functions. Otherwise continuum wave functions have to be calculated separately.

The simplified boundary conditions are especially important for the three positively charged particles where otherwise the non-scaled boundary condition involves complicated functions with slow asymptotic convergence.

The drawbacks of the complex scaling method is first that it requires the numerically slower complex arithmetics to be used and second that the ranges of short-range potentials effectively become larger after complex scaling with the numerically stronger demand of more accurate treatment at larger distances.

We have illustrated the viability of the method by applications to three systems, one benchmark model system and two realistic systems, one with short-range potentials and the other in addition also including the long-range Coulomb potentials. In conclusion the complex-scaled hyper-spheric approach to Faddeev equations is a viable alternative method for calculating three-body resonances and continuum spectrum states.

References

1. H.A. Bethe and E.E. Salpeter, *Quantum mechanics of one- and two-electron atoms*, Springer Verlag, Berlin/New York, (1957).
2. E. Nielsen, D.V. Fedorov, A.S. Jensen, and E. Garrido, *Phys. Rep.* **347**, 373 (2001)
3. L.D. Faddeev, *Sov. Phys. JETP* **12**, 1014 (1961)
4. J. Macek, *J. Phys.* **B1**, 831 (1968)

5. D.V. Fedorov, E. Garrido, and A.S. Jensen, Phys. Rev. **C51**, 3052 (1995)
6. E. Garrido, D.V. Fedorov, and A.S. Jensen, Europhys. Lett. **43**, 386 (1998)
7. E. Garrido, D.V. Fedorov, and A.S. Jensen, Nucl. Phys. A **695**, 109 (2001)
8. J. Aguilar and J.M. Combes, Commun. Math. Phys. **22**, 169 (1971)
9. E. Balslev and J.M. Combes, Commun. Math. Phys. **22**, 280 (1971)
10. Y.K. Ho, Phys. Rep. **99**, 1 (1983)
11. A. T. Kruppa, R. G. Lovas, and B. Gyarmati, Phys. Rev. **C37**, 383 (1988)
12. N. Moiseyev, Phys. Rep. **302**, 212 (1998)
13. A. Csoto, Few Body Syst. Suppl. **13**, 111 (2000)
14. H.Witala and W.Glockle, Phys.Rev. **C60**, 024002 (1999)
15. E. A. Kolganova, A. K. Motovilov, and Y. K. Ho, Nucl. Phys. **A684**, 623c (2001)
16. T. Myo, K. Kato, S. Aoyama, and K. Ikeda, Phys. Rev. **C63**, 054313 (2001)
17. T.Alferova, S.Andersson, N.Elander, S.Levin, and E.Yarevsky, Few-Body Systems **31**, 177 (2002)
18. D.V. Fedorov and A.S. Jensen, Phys. Lett. **B 389**, 631 (1996)
19. D.V. Fedorov and A.S. Jensen, Phys. Rev. Lett. **71**, 4103-4106 (1993)
20. D.V.Fedorov and A.S.Jensen, J. Phys. A, **34**, 6003 (2001); Nucl. Phys. **A697**, 783 (2002)
21. A.Cobis, D.V.Fedorov and A.S.Jensen, Phys.Rev.Lett. **79**, 2411 (1997); Phys.Rev. **C58**, 1403 (1998)
22. Aizenberg-Selov, Nucl. Phus. **A506**, 1 (1990)